

Article

Above Room Temperature Reversible Phase Transition Induces Distinct Dielectric and Nonlinear Optical Switching Response Behavior in Crown-Ether-Based Supramolecular Clathrate

Jing Jing ¹, Fan Jiang ¹, Yan-Li Wei ¹, Chao Shi ², Heng-Yun Ye ² and Yi Zhang ^{1,2,*}

¹ Ordered Matter Science Research Center, Jiangsu Key Laboratory for Science and Applications of Molecular Ferroelectrics, Southeast University, Nanjing 211189, China; 220162415@seu.edu.cn (J.J.); 220172879@seu.edu.cn (F.J.); 220162392@seu.edu.cn (Y.-L.W.)

² Chaotic Matter Science Research Center, Jiangxi University of Science and Technology, Ganzhou 341000, China; shic@jxust.edu.cn (C.S.); yehy@jxust.edu.cn (H.-Y.Y.)

* Correspondence: yizhang1980@seu.edu.cn

Received: 27 February 2019; Accepted: 27 March 2019; Published: 1 April 2019



Abstract: Stimuli-responsive materials with coexisting nonlinear optical (NLO) and dielectric properties are technologically important, which enable simultaneous conversion of optoelectronic properties between different states under external stimuli. By rationally screening guest cations (C₆H₅NF₂)⁺ in the crown-ether inclusion system, we synthesized a crown-ether supramolecular compound [(C₆H₅NF₂)(18-crown-6)][PF₆] (**1**). Differential scanning calorimetry (DSC) showed that **1** undergoes a reversible phase transition above room temperatures (305 K/292 K), with a thermal hysteresis of 13 K. Temperature-dependent dielectric and NLO measurements show that the compound exhibits two distinct switching response behaviors. Structural analysis indicates that the order–disorder change of the host molecule 18-crown-6 and the guest organic cation during the phase transition induces the dielectric and NLO switching behavior of the compound.

Keywords: optical-electrical duple switch; phase transition; host-guest inclusion

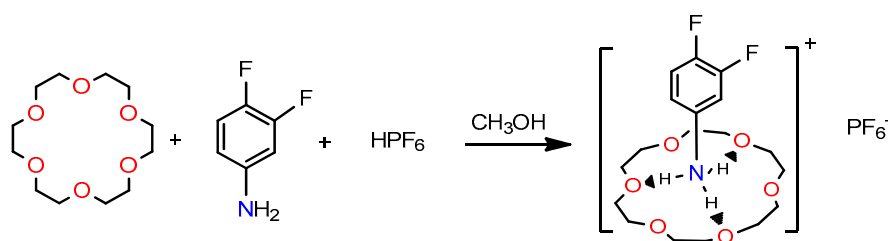
1. Introduction

As an important class of functional materials, compounds with switchable physical properties via optical, electrical, magnetic, or mechanical manipulation are technologically important, because they can be used in a wide range of applications, including switches and memory devices [1–5]. Recently, a great deal of effort in this field has been devoted to the design of molecule-based materials with multiple switching effects of physical properties for potential application in the fields of digital processing, optoelectronic devices, and sensors [6–8]. Among them, crown-ether-based rotator-stator-type supramolecular compounds have shown advantages in realization of such effects [9–13]. This is due to the structural characteristics of the supramolecular compounds, where the dipolar rotator molecules easily undergo the order–disorder change, leading to rich structural phase transitions accompanied by ferroelectric, dielectric, and nonlinear optical (NLO) switching, as exemplified by [(C₇H₁₀NO)(18-crown-6)][BF₄], [(DIPA)(18-crown-6)][ClO₄] (DIPA = 2,6-diisopropylanilinium cation), [(DPA)(18-crown-6)][ClO₄] (DPA = dipropylamine cation), [(*m*-FAni)(DB-18-crown-6)][Ni(dmit)₂] (*m*-FAni = *m*-fluoroanilinium cation; dmit^{2−} = 2-thioxo-1,3-dithiole-4,5-dithiolate cation), and [(Hcha)(18-crown-6)][ClO₄] (Hcha = protonated cyclohexyl ammonium) [4,14–17].

Although a few novel crown-ether-based clathrates have been synthesized recently, there is still much room for structural tailoring, because (i) the switching behaviors of most of the reported

crown-ether-based clathrates were observed at below room-temperatures, which should be the major obstacle for their practical application, and (ii) most of them crystallize in the centrosymmetric space group, resulting in NLO switching materials of them few [16,18–21].

We recently synthesized a crown ether-based inclusion complex $[(C_6H_5NF_2)(18\text{-crown-6})][ClO_4]$ by tetrahedral anion, which shows dielectric and NLO switching effects simultaneously [22]. As a continuation, we have constructed a new inclusion complex $[(C_6H_5NF_2)(18\text{-crown-6})][PF_6]$ (**1**) based on octahedral anions, in which optical-electrical duple switching properties are realized at above room temperature (Scheme 1). This differs from most of the crown ether inclusion complexes reported, which have a SHG switch response below room temperature [17,23]. Moreover, it is interesting to find that **1** shows a high second harmonic generation (SHG) state in the low temperature phase (LTP) and a low SHG state in the high temperature phase (HTP), totally different from that observed for the previous compound $[(C_6H_5NF_2)(18\text{-crown-6})][ClO_4]$. Herein, we report the synthesis, structural phase transitions, dielectric, and NLO switching effects of **1**.



Scheme 1. Synthesis process and structural diagrams of **1**.

2. Results

2.1. Thermal Properties of **1**

Differential Scanning Calorimetry (DSC) measurement was performed on **1** to detect their phase transition behaviors and confirm transition temperatures (T_c). From this, **1** shows a pair of endo-/exothermic peaks at 305/292 K ($T_{tr}(\mathbf{1}) = 299$ K) with a large thermal hysteresis of 13 K. We estimate the entropy changes (ΔS) to be 17.62 J/(mol K). According to the Boltzmann's equation $\Delta S = R \ln(N)$, where R is the gas constant, N represents the ratio of the numbers of respective geometrically distinguishable orientations; the calculated values of N is 8.32. These features suggesting that there is a reversible first-order phase transition at $T_{tr}(\mathbf{1})$ (Figure 1). For convenience, the phase above $T_{tr}(\mathbf{1})$ is assigned as the high-temperature phase (HTP) and the phase below $T_{tr}(\mathbf{1})$ as the low-temperature phase (LTP). To explain the phenomenon in microscopic view, the variable-temperature X-ray single-crystal structural analyses are introduced in great detail (see below).

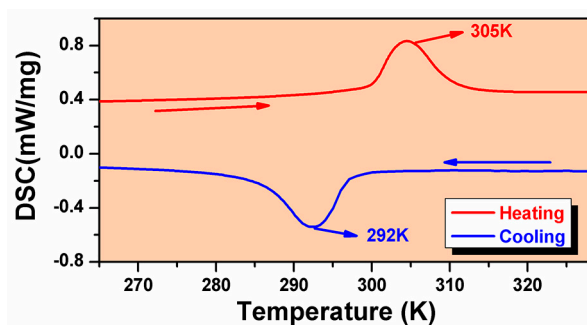


Figure 1. DSC curves of **1**.

2.2. Variable-Temperature Structures of **1**

To systematically investigate the structural phase transitions of **1**, we determined variable-temperature single-crystal structures. They display zero-dimensional cation-anion packing structures (Figure 2b,c and Figure S4). At 293 K in the LTP, **1** crystallizes in the orthorhombic non-centrosymmetric space group $Pna2_1$, with $a = 13.425(3)$ Å, $b = 11.817(2)$ Å, $c = 15.660(3)$ Å, $Z = 4$, $V = 2484.4(8)$ Å³ (Table S1). The asymmetric unit of the crystal structure is comprised of one $[(C_6H_5NF_2)(18\text{-crown-6})]^+$ complex cation and one PF_6^- anion, as shown in Figure 2a. The guest cation sits in the cavity of the 18-crown-6 molecule via N–H···O hydrogen-bonding interactions (for hydrogen bond geometries, see Table S2). All components for compound **1** are ordered. At 293 K, compound $[(C_6H_5NF_2)(18\text{-crown-6})][ClO_4]$ includes the same $[(C_6H_5NF_2)(18\text{-crown-6})]^+$ complex cation and a distinct ClO_4^- anion. The ClO_4^- anion is highly disordered, which is different from compound **1**. As the temperature increases, compound **1** crystallized in the same crystal system and point group, but the space group transforms into the $Cmc2_1$ at 323 K of the HTP, with $a = 11.9791(10)$ Å, $b = 13.6041(12)$ Å, $c = 15.4202(8)$ Å, $Z = 4$, $V = 2513.0(3)$ Å³ (Table S1). The $[(C_6H_5NF_2)(18\text{-crown-6})]^+$ complex cation undergoes a transition from order state to disorder state (Figure 2b). The 18-crown-6 macrocycle is modeled with two orientations having the same occupancy of 0.5. For the 3,4-difluoroanilinium group, the meta F atom is distributed over two positions with a site occupancy ratio of 1:1. The N–H···O hydrogen bond geometries show no obvious changes (Table S2). This is diverse, with the change of compound $[(C_6H_5NF_2)(18\text{-crown-6})][ClO_4]$ from the orthorhombic system in LTP to the monoclinic system in HTP. Therefore, we believe that the interaction between different anions and the same cations may be diverse, leading to diversities in physical properties.

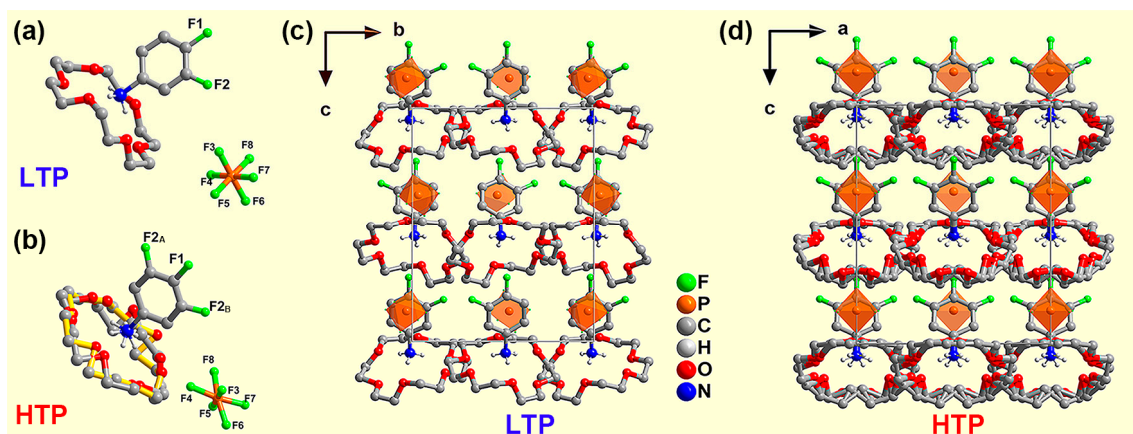


Figure 2. (a) The asymmetric units of **1** in low-temperature phase (LTP). (b) The asymmetric units of **1** in high-temperature phase (HTP). The disordered parts in (b) are distinguished by different bond colors. (c) The crystallographic packing diagrams of **1** in LTP. (d) The crystallographic packing diagrams of **1** in HTP.

2.3. Dielectric Properties of **1**

Testing the dielectric permittivity of a compound can systematically investigate whether the compound is a phase transition material. The temperature dependence of ϵ' (the real part of the complex dielectric permittivity, $\epsilon = \epsilon' - i\epsilon''$, where ϵ'' is the imaginary part) at selected frequencies was tested on the polycrystalline samples. As shown in Figure 3a, obvious step-like dielectric anomalies were found at the $T_{tr}(\mathbf{1})$ in the heating run, and it was also shown that the phase transition temperature of **1** is independent of the various frequencies. However, the value of ϵ' is sensitive to frequency, and the dielectric constant gradually increases with the decrease of frequency, which demonstrates the general characteristics of dielectric materials. As exhibited in Figure 3b, the real component ϵ' shows a step-like increase from 4.10 to 6.65 at around $T_{tr}(\mathbf{1})$ in the heating and cooling modes at 100 kHz, and the high dielectric state (ON) is about 1.62 times greater than that of the low dielectric state (OFF).

The reversible dielectric anomalies observed from **1** correspond to the results of DSC. The reversible switching behavior between the corresponding low- and high-dielectric states is demonstrated for a powder-pressed pellet at 100 kHz in several sequential cycles (Figure 3c). Within a few runs, the dielectric signal between the corresponding switch “ON” and switch “OFF” remains essentially unchanged. The mentioned results show that **1** exhibits excellent dielectric switching characteristics above room-temperature, making it promising for the stimuli-responsive or solid-state materials.

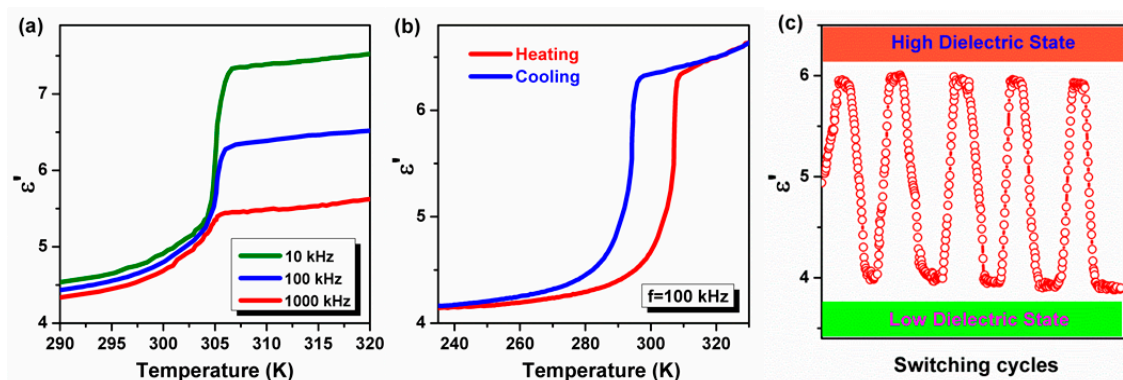


Figure 3. (a) Temperature-dependence of the real part (ϵ') of the polycrystalline sample for **1** at selected frequencies in the heating run. (b) Temperature-dependence of the real part (ϵ') of the polycrystalline sample for **1** at 100 kHz in the heating-cooling run. (c) The recoverable switching of dielectric effects of compound **1**.

2.4. SHG Properties of **1**

NLO activity measurement for sieved crystalline samples reveals that **1** has a macroscopic SHG-active response. The relationship between particle size and SHG response at 298 K is shown in Figure 4a—the larger particle size, the higher the SHG intensity. This indicates that they are of phase-matching NLO materials. The temperature-dependent SHG effect of compound **1** was then measured (Figure 4b). In the LTP, compound **1** has a high SHG-active response state, approximately 0.4 times as large as that of KH_2PO_4 (KDP). This response is small in comparison with those of existing excellent SHG materials, but moderate in comparison with those of existing analogous crown-ether compounds [14]. With the temperature increasing to HTP, SHG intensity **1** suddenly decreases to 0.34 times that of KDP, showing another low SHG response state. Considering that SHG coefficient for polar materials is the function of the spontaneous polarization, we estimated the polarization of **1** by using the point charge models to understand the contrary switching effects (Tables S3 and S4). For **1**, as the space group changes from $Pna2_1$ to $Cmc2_1$, the spontaneous polarization is reduced from $12.9 \mu\text{C}/\text{cm}^2$ to $12.2 \mu\text{C}/\text{cm}^2$, which may lead to the decrease of SHG signal. Moreover, a recoverable switching effect of the SHG was examined. The intensity and the switching period of the SHG signals remain virtually unchanged after many switching cycles (Figure 4c). These make them promising candidates in the field of SHG switches.

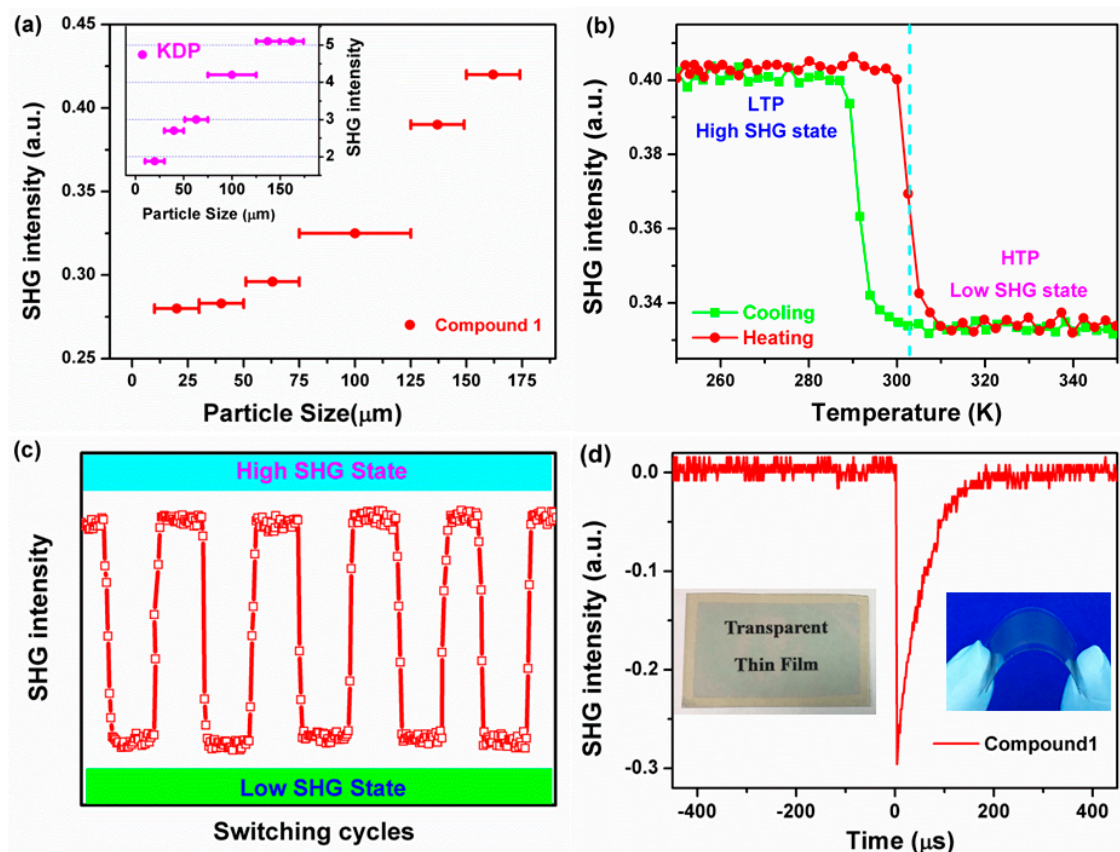


Figure 4. (a) Particle size versus second harmonic generation (SHG) intensity data of the 1 and KH_2PO_4 (KDP) single crystal at 298 K. (b) Temperature dependency of SHG effects of 1 in the heating run at the 125 μm particle size. (c) The NLO switching trajectory from high- to low-state of 1. (d) Oscilloscope trace of the SHG of thin film. Inset: flexibility of the thin film.

2.5. The Flexible Thin Films of 1

In order to further explore more attractive practical applications, we tried to grow films on flexible substrates. The fabricated thin films on the flexible substrates are transparent, flexible, and not fragile; they can be bent by applying external forces, indicating good mechanical property (Figure 4d). Attractively, similar to crystalline samples, thin films also show the NLO effects (Figure 4d). By changing the rotational speed, thin films with 1 μm , 850 nm, and 750 nm thicknesses were prepared and measured by atomic force microscopy (AFM). By comparing the SHG signal intensity of films with different thickness, we find that the SHG signal increases with the increase of film thickness (Figure S5). This will surely improve its application in optoelectronic devices in the future.

3. Experiment Section

3.1. Preparation of Crystals and Thin Films

All analytical grade chemicals were purchased from Energy Chemical and used without further purification. Colorless block crystals of 1 were obtained by the slow evaporation of the methanol solution containing 3,4-difluoroaniline, HPF_6 , and 18-crown-6 with 1:1:1 molar ratio (Figure S1). The phase purity of 1 was confirmed by IR spectra (Figure S2) and PXRD (powder X-ray diffraction) pattern at room temperature (Figure S3). The transparent thin films for 1 were fabricated on a flexible substrate of polyethylene terephthalate (Figure 4d). The single-phase compound 1 was dissolved in DMF to form a saturated solution having a solubility of about 40%. Polyethylene terephthalate (PET) substrates were treated by Digital UV Ozone System for half an hour, and then 1–2 layers of the films were repeatedly deposited on the substrates. Through a convenient and inexpensive spin-coating

approach with rotary speeds of 3000, 4000, and 6000 rev/min, dendrite growth was induced on the substrates to form single crystal thin films. The spin-coating films were annealed at 353K for one hour. The thickness of the films were about 1 μm , 850 nm, and 750 nm by measuring the artificial gap with an atomic force microscope (AFM).

3.2. Single-Crystal X-ray Crystallography

Variable-temperature X-ray diffraction was collected with Mo-K α radiation ($\lambda = 0.71073 \text{ \AA}$) on a Rigaku Saturn 724 diffractometer equipped with gas spray cooler device. The direct methods were used to solve the structures and the full-matrix least-squares methods on F^2 were also introduced to refine the structures by using SHELXLTL-2014 software package. The non-hydrogen atoms were refined anisotropically using all the reflections with $I > 2\sigma(I)$. The hydrogen atoms were added geometrically at idealized positions and refined with the “riding” model. Crystallographic data, structure refinements, and details of the data collection of **1** are summarized in Table S1.

3.3. General Measurements

The infrared (IR) spectra was recorded by a Nicolet 5700 spectrometer. PXRD measurements were performed on a Rigaku D/MAX 2000 PC X-ray diffractometer instrument in the 2θ range of 5° – 50° with a step size of 0.02° . Differential scanning calorimetry (DSC) measurements were implemented using a NETZSCH instrument with a rate of 5 K min^{-1} in N_2 flow and a temperature range of 220 K to 328 K for **1**. Dielectric measurements were performed on a Tonghui TH2828A instrument between 230 K and 350 K over a frequency range from 80 kHz to 1 MHz with an applied electric field of 1 V. The SHG measurements were collected on an Ins 1210058, INSTEC Instrument with the laser Vibrant 355 II, OPOTEK (pulsed Nd: YAG at a wavelength of 1064 nm, 1.6 MW peak power, 5 ns pulse duration, 10 Hz repetition rate).

4. Conclusions

In summary, we have successfully synthesized a new crown-ether supramolecular inclusion compound $[(\text{C}_6\text{H}_5\text{NF}_2)(18\text{-crown-6})][\text{PF}_6]$ with a solid state reversible phase transition above room temperature. Crystal structure analysis reveals that it undergoes a reversible structural phase transition from the polar space group of $Pna2_1$ to the polar space group $Cmc2_1$, induced by the order-disorder change of the host molecule 18-crown-6 and the guest organic cation. This change in crystal structure results in compound **1** exhibiting different dielectric and NLO switching response behavior. Compound **1** shows the high SHG state in the LTP and the low SHG state in the HTP, whereas **1** presents the low dielectric state in the LTP and high dielectric state in the HTP. The contrary switching effects in **1** should expand application areas of dielectric and NLO dual switch. These results will surely provide new impetus for the design of novel multifunctional stimuli-responsive materials based on crown-ether host-guest supramolecular clathrates.

Supplementary Materials: The following are available online at <http://www.mdpi.com/2073-4352/9/4/184/s1>, CCDC 1847880, 1847883, Figure S1: Crystal morphology of **1**. Figure S2: IR spectra of **1**. Figure S3: PXRD patterns of **1** measured at room temperature. Figure S4: The packing diagrams of **1** at (a) 293 K and (b) 323 K. Hydrogen atoms in were omitted for clarity. Table S1: Crystallographic Data for compound **1**. Table S2: Hydrogen bonds (\AA , $^\circ$) for **1**. Table S3: Calculation of the polarization of **1** (293 K) with a point charge model. Table S4: Calculation of the polarization of **1** (323 K) with a point charge model.

Author Contributions: Conceptual design experiments, J.J., F.J., Y.-L.W., and Y.Z.; data analysis, C.S. and H.-Y.Y.; the manuscript was written through contributions of all authors.

Acknowledgments: This work was supported by the National Key Research and Development Program of China (Grant 2017YFA0204800), the National Natural Science Foundation of China (21522101), and the Fundamental Research Funds for the Central Universities (Grant 2242017K41027).

Conflicts of Interest: The authors declare no conflict of interest.

References

1. Zhang, S.-Y.; Li, J.; Zeng, Y.; Wen, H.-R.; Du, Z.-Y. Hydrogen-bond-directed assemblies of [La(18-crown-6)(H₂O)₄](BiCl₆)·3H₂O and [Nd(18-crown-6)(H₂O)₄](BiCl₆)·3.5H₂O regulated by different symmetries. *J. Mol. Struct.* **2016**, *1125*, 227–233. [[CrossRef](#)]
2. Shi, C.; Zhang, X.; Cai, Y.; Yao, Y.-F.; Zhang, W. A chemically triggered and thermally switched dielectric constant transition in a metal cyanide based crystal. *Angew. Chem. Int. Ed. Engl.* **2015**, *54*, 6206–6210. [[CrossRef](#)]
3. Sun, X.-F.; Wang, Z.-X.; Li, P.-F.; Liao, W.-Q.; Ye, H.-Y.; Zhang, Y. Tunable dielectric responses triggered by dimensionality modification in organic-inorganic hybrid phase transition compounds (C₅H₆N)Cd_nCl_{2n+1} (n = 1 and 2). *Inorg. Chem.* **2017**, *56*, 3506–3511. [[CrossRef](#)]
4. Akutagawa, T.; Koshinaka, H.; Sato, D.; Takeda, S.; Noro, S.; Takahashi, H.; Kumai, R.; Tokura, Y.; Nakamura, T. Ferroelectricity and polarity control in solid-state flip-flop supramolecular rotators. *Nat. Mater.* **2009**, *8*, 342–347. [[CrossRef](#)]
5. Liao, W.-Q.; Ye, H.-Y.; Fu, D.-W.; Li, P.-F.; Chen, L.-Z.; Zhang, Y. Temperature-triggered reversible dielectric and nonlinear optical switch based on the one-dimensional organic-inorganic hybrid phase transition compound [C₆H₁₁NH₃]₂CdCl₄. *Inorg. Chem.* **2014**, *53*, 11146–11151. [[CrossRef](#)]
6. Li, W.; He, C.-T.; Zeng, Y.; Ji, C.-M.; Du, Z.-Y.; Zhang, W.-X.; Chen, X.-M. Crystalline supramolecular gyroscope with a water molecule as an ultrasmall polar rotator modulated by charge-assisted hydrogen bonds. *J. Am. Chem. Soc.* **2017**, *139*, 8086–8089. [[CrossRef](#)]
7. Sun, Z.-H.; Luo, J.-H.; Chen, T.-L.; Li, L.-N.; Xiong, R.-G.; Tong, M.-L.; Hong, M.-C. Distinct molecular motions in a switchable chromophore dielectric 4-N,N-Dimethylamino-4'-N'-methylstilbazolium Trifluoromethanesulfonate. *Adv. Funct. Mater.* **2012**, *22*, 4855–4861. [[CrossRef](#)]
8. Cai, H.-L.; Zhang, Y.; Fu, D.-W.; Zhang, W.; Liu, T.; Yoshikawa, H.; Awaga, K.; Xiong, R.-G. Above-room-temperature magnetodielectric coupling in a possible molecule-based multiferroic: triethylmethylammonium tetrabromoferrate(III). *J. Am. Chem. Soc.* **2012**, *134*, 18487–18490. [[CrossRef](#)]
9. Liu, Y.; Zhu, C.-L.; Qin, L.-L.; Zheng, X.-Y.; Liu, Z.-Q. Anisotropic dielectric phase transition triggered by pendulum-like motion coupled with proton transfer in a layered hybrid crystalline material (4-nitroanilinium⁺) (18-crown-6) (H₂PO₄⁻) (H₃PO₄)₂. *J. Mol. Struct.* **2018**, *1164*, 556–562. [[CrossRef](#)]
10. Chen, Y.; Liu, Y.; Gao, B.-Z.; Zhu, C.-L.; Liu, Z.-Q. Inorganic anions regulate the phase transition in two organic cation salts containing [(4-Nitroanilinium)(18-crown-6)]⁺ supramolecules. *Crystals* **2017**, *7*, 224. [[CrossRef](#)]
11. Zhu, C.-L.; Liu, Y.; Wang, K.; Chen, Y.; Liu, Z.-Q. Crystal structure and phase transition of the C–H···F–H-bonded supramolecular compound with 4-nitroanilinium based on 18-crown-6. *Crystals* **2017**, *7*, 276.
12. Tang, Y.-Z.; Yu, Y.-M.; Xiong, J.-B.; Tan, Y.-H.; Wen, H.-R. Unusual high-temperature reversible phase-transition behavior, structures, and dielectric-ferroelectric properties of two new crown ether clathrates. *J. Am. Chem. Soc.* **2015**, *137*, 13345–13351. [[CrossRef](#)]
13. Nishihara, S.; Akutagawa, T.; Hasegawa, T.; Fujiyama, S.; Nakamura, T.; Nakamura, T. Two polymorphs of (anilinium)(18-Crown-6)[Ni(dmit)₂]: Structure and magnetic properties. *J. Solid State Chem.* **2002**, *168*, 661–667. [[CrossRef](#)]
14. Fu, D.-W.; Zhang, W.; Cai, H.-L.; Zhang, Y.; Ge, J.-Z.; Xiong, R.-G.; Huang, S.D. Supramolecular bola-like ferroelectric: 4-methoxyanilinium tetrafluoroborate-18-crown-6. *J. Am. Chem. Soc.* **2011**, *133*, 12780–12786. [[CrossRef](#)]
15. Zhang, Y.; Ye, H.-Y.; Fu, D.-W.; Xiong, R.-G. An order-disorder ferroelectric host-guest inclusion compound. *Angew. Chem. Int. Ed. Engl.* **2014**, *53*, 2114–2118. [[CrossRef](#)]
16. Tang, Y.-Z.; Gu, Z.-F.; Xiong, J.-B.; Gao, J.-X.; Liu, Y.; Wang, B.; Tan, Y.-H.; Xu, Q. Unusual sequential reversible phase transitions containing switchable dielectric behaviors in cyclopentyl ammonium 18-crown-6 perchlorate. *Chem. Mater.* **2016**, *28*, 4476–4482. [[CrossRef](#)]
17. Ji, C.-M.; Sun, Z.-H.; Zhang, S.-Q.; Zhao, S.-G.; Chen, T.-L.; Tang, Y.-Y.; Luo, J.-H. A host-guest inclusion compound for reversible switching of quadratic nonlinear optical properties. *Chem. Commun.* **2015**, *51*, 2298–2300. [[CrossRef](#)]

18. Chen, C.; Wang, F.-F.; Zhang, Y.; Ye, Q.; Ye, H.-Y.; Fu, D.-W. A high-temperature supramolecular-based switchable dielectric material with electrical bistability between high and low dielectric states. *CrystEngComm* **2015**, *17*, 2479–2485. [[CrossRef](#)]
19. Li, P.-F.; Liao, W.-Q.; Zhou, Q.-Q.; Ye, H.-Y.; Zhang, Y. Inorganic anion regulated phase transition in a supramolecular adduct: 4-trifluoromethoxyanilinium hexafluorophosphate-18-crown-6. *Inorg. Chem. Commun.* **2015**, *61*, 77–81. [[CrossRef](#)]
20. Khan, T.; Asghar, M.A.; Sun, Z.-H.; Zeb, A.; Ji, C.-M.; Luo, J.-H. A supra-molecular switchable dielectric material with non-linear optical properties. *J. Mater. Chem. C* **2017**, *5*, 2865–2870. [[CrossRef](#)]
21. Fu, D.-W.; Zhang, Y.; Cai, H.-L.; Zhu, H.-M.; Chen, X.-Y.; Xiong, R.-G. The first example of a molecule-based ferroelectric with barium cation: Catena-(μ 2-nitrito-O,O)-bi-aqua-(18-crown-6)-barium nitrite. *J. Mater. Chem.* **2012**, *22*, 17525–17530. [[CrossRef](#)]
22. Wei, Y.-L.; Jing, J.; Shi, C.; Ye, H.-Y.; Wang, Z.-X.; Zhang, Y. Unusual high-temperature reversible phase transition containing dielectric and nonlinear optical switches in host-guest supramolecular crown ether clathrates. *Chem. Commun.* **2018**, *54*, 8076–8079. [[CrossRef](#)]
23. Sun, Z.; Li, S.; Zhang, S.; Deng, F.; Hong, M.; Luo, J. Second-order nonlinear optical switch of a new hydrogen-bonded supramolecular crystal with a high laser-induced damage threshold. *Adv. Opt. Mater.* **2014**, *2*, 1199–1205. [[CrossRef](#)]



© 2019 by the authors. Licensee MDPI, Basel, Switzerland. This article is an open access article distributed under the terms and conditions of the Creative Commons Attribution (CC BY) license (<http://creativecommons.org/licenses/by/4.0/>).